

PAPER • OPEN ACCESS

## Low-index quantum-barrier single-pass tapered semiconductor optical amplifiers for efficient coherent beam combining

To cite this article: P Albrodt *et al* 2020 *Semicond. Sci. Technol.* **35** 065018

View the [article online](#) for updates and enhancements.



**ECS** The Electrochemical Society  
Advancing solid state & electrochemical science & technology  
2021 Virtual Education

### Intensive Short Courses

Sun, Oct 10 & Mon, Oct 11

Providing students and professionals with in-depth education on a wide range of topics

Early registration deadline: Sep 13, 2021

Register early and save!

# Low-index quantum-barrier single-pass tapered semiconductor optical amplifiers for efficient coherent beam combining

P Albrodt<sup>1</sup>, M Niemeyer<sup>2</sup>, M Elattar<sup>2</sup> , J Hamperl<sup>1</sup>, G Blume<sup>2</sup>, A Ginolas<sup>2</sup>, J Fricke<sup>2</sup>, A Maaßdorf<sup>2</sup>, P Georges<sup>1</sup>, G Lucas-Leclin<sup>1</sup> , K Paschke<sup>2</sup> and P Crump<sup>2,3</sup> 

<sup>1</sup> Université Paris-Saclay, Institut d'Optique Graduate School, CNRS, Laboratoire Charles Fabry, 91127, Palaiseau, France

<sup>2</sup> Ferdinand-Braun-Institut, Leibniz-Institut für Höchstfrequenztechnik, Gustav-Kirchhoff Str. 4, Berlin D-12489 Germany

E-mail: [paul.crump@fbh-berlin.de](mailto:paul.crump@fbh-berlin.de)

Received 16 January 2020, revised 26 February 2020

Accepted for publication 16 March 2020

Published 19 May 2020



## Abstract

The requirements for coherent combination of high power GaAs-based single-pass tapered amplifiers are studied. Changes to the epitaxial layer structure are shown to bring higher beam quality and hence improved combining efficiency for one fixed device geometry. Specifically, structures with large vertical near field and low wave-guiding from the active region show 10% higher beam quality and coherent combining efficiency than reference devices. As a result, coherent combining efficiency is shown to be limited by beam quality, being directly proportional to the power content in the central lobe across a wide range of devices with different construction. In contrast, changes to the in-plane structure did not improve beam quality or combining efficiency. Although poor beam quality does correlate with increased optical intensities near the input aperture, locating monolithically-integrated absorption regions in these areas did not lead to any performance improvement. However, large area devices with subsequently improved cooling do achieve higher output powers. Phase noise can limit coherent combining, but this is shown to be small and independent of device design. Overall, tapered amplifiers are well suited for high power coherent combining applications.

Keywords: semiconductor optical amplifier, high power, conversion efficiency, coherent beam combination, beam quality, quantum well design

(Some figures may appear in colour only in the online journal)

## 1. Introduction

GaAs-based high power diode lasers are key components for commercial laser systems, and continuous improvements in their brightness is sought, in terms of watts of optical output

per solid angle of emission [1, 2]. Sources with narrow spectral width  $\Delta\lambda_{95\%}$  are preferred, for pumping narrow lines, for spectroscopy and sensing applications such as LIDAR, and for later spectral combining via a grating for further enhanced brightness [2]. Coherent combining is a technique that allows the emission from many semiconductor sources to be combined within a single beam, scaling optical output power  $P_{\text{opt}}$  delivered within a narrow spectral line without degrading beam quality, so has high potential for use in a variety of optical systems [2]. Coherent combining can be performed by actively regulating the phase of each element, as studied

<sup>3</sup> Author to whom any correspondence should be addressed.



Original content from this work may be used under the terms of the [Creative Commons Attribution 4.0 licence](https://creativecommons.org/licenses/by/4.0/). Any further distribution of this work must maintain attribution to the author(s) and the title of the work, journal citation and DOI.

here. Alternatively, the phase can be tied together using various passive techniques, as reviewed recently in [3, 4]. In previous studies, the authors have shown that single-pass tapered semiconductor amplifiers with  $P_{\text{opt}} = 4 \dots 5$  W can be efficiently coherently combined using active phase control into beams with  $P_{\text{opt}} > 20$  W, in continuous wave (CW) and quasi-continuous wave (QCW) mode, and used to generate high intensities of green light, using frequency conversion techniques [5–7]. These previous studies primarily focused on developing techniques for the effective coherent combining of tapered amplifiers.

In contrast, we review here the impact of changes in the device design and construction on tapered amplifiers operating close to a wavelength  $\lambda = 976$  nm. In studies by other groups, active coherent combining has been successfully performed in large arrays of ridge waveguide amplifiers that are limited to a single optical mode by design, through the use of a well-defined lateral waveguide [8, 9]. Such systems are restricted to around 1 W per emitter. In contrast, tapered amplifiers that use various different designs can deliver diffraction limited power  $P_{\text{DL}} = 5 \dots 10$  W in CW mode,  $P_{\text{DL}} > 15$  W in QCW mode (100  $\mu\text{s}$ ) [10] and  $P_{\text{DL}} > 70$  W for  $< 10$  ps wide pulses [11], enabling higher overall power levels per device, for large reductions in size, complexity and cost. However, tapered amplifiers typically are fabricated with more than  $50 \times$  larger surface area than a comparable ridge waveguide laser, and do not include any lateral waveguiding, meaning they are potentially more susceptible to the onset of instabilities such as filamentation [12, 13] that could lead to phase instability or degraded coherent combining efficiency. In recent studies on modern, low-defect broad area lasers, experimental and theoretical studies find little indication for filamentation playing a significant role in their beam properties [13–16]. Coherent combination is however a more demanding application.

In previous work by the authors on single-pass tapered amplifiers, both higher overall  $P_{\text{DL}}$  and a higher fraction of nearly diffraction limited emission  $\eta_{\text{CL}} = P_{\text{DL}}/P_{\text{tot}}$  was sought, where  $P_{\text{tot}}$  is the total spatially integrated optical output power. Higher  $P_{\text{DL}}$  and  $\eta_{\text{CL}}$  was achieved by using epitaxial layer designs with low confinement factor in the active region  $\Gamma$  for low modal gain factor  $\Gamma g_0$  and extremely low vertical divergence angle,  $\Theta_{\text{V}}^{95\%}$  (with 95% power content) [10, 17]. The use of an active region containing low-index quantum barriers (LIQB) was also proposed as being beneficial, as this potentially limits the impact of any variation in refractive index of the active region (due to oscillations in carrier density or temperature) on the propagating field [10]. In addition, devices with larger surface areas were found to achieve higher overall power and hence higher  $P_{\text{DL}}$  due to their better cooling [10]. Similar results were reported in free-standing tapered lasers [18].

Following these studies, we present here a comparison of the impact of epitaxial layer design and lateral (in-plane) structuring on the performance of tapered amplifiers in coherent combination, for a fixed coherent combination scheme taken from [5, 6]. We start with an analysis of the impact of epitaxial layer structure, first quantifying the impact of LIQB on lateral waveguiding in simulation. We then fabricate and

test comparable tapered amplifiers using two related epitaxial layer designs, one extremely low divergence (ELoD) design that uses LIQB and one similar reference design without LIQB, and show that the beam quality and coherent combining efficiency in ELoD-based amplifiers is improved. We next analyze the impact of changes in the lateral (in-plane) design for ELoD-based amplifiers, increasing surface area, seeking higher powers (following [10]), and implementing absorber regions around the input aperture (following [19]), seeking improved beam quality and  $P_{\text{DL}}$ . We then conclude with an overview, showing that the coherent combining efficiency correlates directly to  $P_{\text{DL}}/P_{\text{tot}}$ , independent of vertical and lateral device design. We also show that phase noise is low ( $< \lambda/100$ ), and independent of device design, and does not restrict coherent combining. Overall, tapered amplifiers are confirmed to enable reproducible, stable coherent combining, and hence be suitable sources for future compact, efficient laser systems.

## 2. Device configuration

### 2.1. Vertical epitaxial laser design for coherent beam combining (CBC)

Diode lasers using two different vertical layer designs are compared in this paper, both with operating wavelength close to  $\lambda = 976$  nm. A reference design is used, taken from [20], whose active zone (AZ), contains a double InGaAs quantum well with  $\text{GaAs}_x\text{P}_{1-x}$  barriers, where  $x = 80\%$ . The AZ is located asymmetrically within a  $4.8 \mu\text{m}$  thick  $\text{Al}_y\text{Ga}_{1-y}\text{As}$  waveguide, where  $y = 35\%$ . The vertical far field is  $\Theta_{\text{V}}^{95\%} = 46^\circ$  and the near field width is  $W_{95\%} = 2.19 \mu\text{m}$  (at 95% power content) (see figure 1 left). The reference design is compared here to a second design with narrower vertical far field, achieved by using a modified vertical waveguide design for extremely low vertical divergence that makes use of low-index quantum barriers LIQB, as described in [21], specifically the higher performance ‘ELoD2’ variant, taken from [22]. The ELoD2 AZ includes a triple InGaAs quantum well separated by  $\text{GaAs}_x\text{P}_{1-x}$  barriers, with  $x = 0.66$ . The AZ is located asymmetrically within a  $4.8 \mu\text{m}$  thick  $\text{Al}_y\text{Ga}_{1-y}\text{As}$  waveguide, where  $y = 15\%$ . The high phosphorus content in the barriers lowers their refractive index below that of the low-aluminum waveguide, compensating for the high refractive index of the InGaAs wells, and reducing the influence of the AZ on the vertical field, leading to narrower  $\Theta_{\text{V}}^{95\%} = 26^\circ$  and  $W_{95\%} = 3.05 \mu\text{m}$ . The vertical refractive index profile and calculated profile of the first guided optical mode are shown in figure 1 for both structures. Total confinement in the AZ is (by design)  $\Gamma = 1.95 \pm 0.1\%$  in both cases, summed across all wells, with the ELoD2 design compensating for the broader near field by adding an extra quantum well.

Broad area lasers were fabricated for both vertical layer designs using a simplified wafer process to obtain characteristic parameters, by measuring the variation of threshold and slope from a series of unmounted bars in pulsed mode, following [21]. Values are summarized in table 1. The characteristic parameters were similar for both designs, with a modal gain parameter  $\Gamma g_0 = 21 \text{ cm}^{-1}$  and optical loss

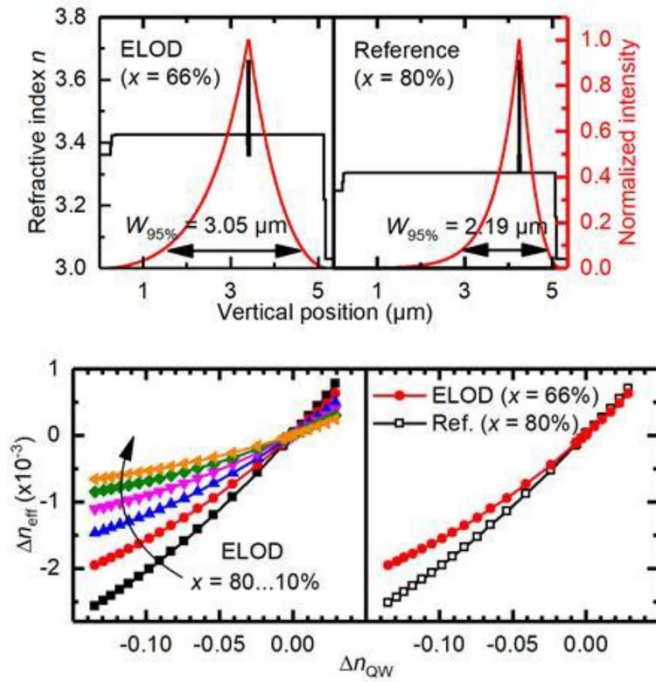


**Figure 1.** Vertical layer designs. Top: Vertical refractive index as function of vertical position and resulting calculated optical intensity profile of the fundamental mode for the two vertical epitaxial layer designs studied here (ELOD and reference). Bottom: Calculated lateral contrast in effective index arising due to variation in the local refractive index of the quantum well, for ELOD and reference designs. In the case of the ELOD design, calculations are repeated for a variation in the composition of the low-index barrier layers located around the quantum well.

$\alpha_i = 0.6 \text{ cm}^{-1}$  for the ELoD2-based lasers and  $\Gamma g_0 = 20 \text{ cm}^{-1}$  and  $\alpha_i = 0.9 \text{ cm}^{-1}$  for the reference material. These parameters lead to a similar overall single-pass peak gain at transparency (amplifier bias equivalent to  $J = J_{\text{transp}}$ ) of  $(\Gamma g_0 - \alpha_i)L_a = 8.2$  and  $7.6$  for an ELoD2 and reference amplifier respectively, for amplifier length of  $L_a = 4 \text{ mm}$ . In the following, we assume that de-tuning from gain peak is small and that differences in the gain spectrum due to changes in the active region play no role. Further studies are needed to confirm this assumption, and to understand the impact of de-tuning.

Both designs show not just comparable peak gain, but also similar internal differential efficiency  $\eta_i > 95\%$ . However, in contrast, the ELoD2 material has increased transparency current density of  $J_{\text{transp}} = 220 \text{ A cm}^{-2}$ , compared to  $J_{\text{transp}} = 137 \text{ A cm}^{-2}$  for the reference material, due to the need to pump three rather than two quantum wells. The lower aluminum concentration in the  $\text{Al}_y\text{Ga}_{1-y}\text{As}$  waveguide in the ELoD2 structure leads to higher electron and hole mobility which also reduces the electrical resistance.

As noted in [10], the use of LIQBs will reduce the impact of oscillations in carrier density and temperature in the AZ on the optical field. Following [23], the refractive index  $n$  of the AZ varies approximately with temperature at a rate of  $dn/dT \sim 2.4 \times 10^{-4} \text{ K}^{-1}$ , and with carrier density  $n_c$ , at a rate of  $dn/dn_c \sim 10^{-20} \text{ cm}^3$ , so that oscillations in local temperature and carrier density of  $\Delta T = 40 \text{ K}$  and  $\Delta n_c = 10^{18} \text{ cm}^{-3}$

**Table 1.** Measured characteristic device parameters and resulting calculated expected single pass net gain at transparency for the two epitaxial layer designs studied here. The measured internal differential efficiency was  $\eta_i > 95\%$  in both cases.

Layer Design	Modal gain parameter $\Gamma g_0$ ( $\text{cm}^{-1}$ )	Optical loss, $\alpha_i$ ( $\text{cm}^{-1}$ )	Transparency current density, $J_{\text{transp}}$ ( $\text{A cm}^{-2}$ )	Single pass net gain at transparency $(\Gamma g_0 - \alpha_i)L_a$ ( $L_a = 4 \text{ mm}$ )
Reference	20	0.9	137	7.6
ELoD2	21	0.6	220	8.2

in the quantum well respectively would lead to oscillations in the refractive index of around  $\Delta n_{\text{QW}} \sim 0.01$ . These oscillations can potentially arise spontaneously in semiconductor amplifiers [12]. Significant local variation in carrier density also occurs due to current spreading and non-clamping at the edges of the injection region, where lateral carrier accumulation is seen in both simulation and measurement [24, 25]. We quantify the potential impact of such oscillations on lateral wave guiding here by calculating the vertical effective index  $n_{\text{eff}}$  of the fundamental mode as a function of the refractive index of the quantum well and figure 1 (right) shows the variation in effective index  $\Delta n_{\text{eff}}$  as a function of change in refractive index of the quantum well  $\Delta n_{\text{QW}}$ , for a well thickness of  $8.5 \text{ nm}$ . The calculations are repeated for the ELoD2 design for  $\text{GaAs}_x\text{P}_{1-x}$  barriers with  $x = 10\% \dots 80\%$ . Reducing  $x$  from  $80\%$  (no LIQB effect, black solid squares) to  $66\%$  (strong negative step in index, structure ‘as grown’, red solid circles), reduces the impact on  $\Delta n_{\text{eff}}$  by around  $20\%$  within the simulated range of  $\Delta n_{\text{QW}}$ , with  $x = 10\%$  reducing the impact around four-fold. The calculation was then repeated for the reference design (with  $y = 35\%$  in the  $\text{Al}_y\text{Ga}_{1-y}\text{As}$  waveguide, but the same well thickness) and this is directly compared to the ‘as grown’ ELoD2 design in figure 1. The ELoD2 design reduces the impact of variation in quantum well refractive index on  $\Delta n_{\text{eff}}$  by around  $15\%$  when compared directly to the baseline design. Overall, the ELoD2 design has lower sensitivity to index variations than the baseline and larger vertical near field at the price of higher threshold current. We expect that this should result in a lower sensitivity to beam filamentation in the lateral profile and hence higher beam quality, as will be investigated in the following section.

## 2.2. Lateral (in-plane) tapered amplifier design

Epitaxial wafers to ELoD2 and reference designs were grown using metalorganic vapor phase epitaxy, and processed using standard techniques into tapered amplifiers, following [10, 17, 20]. The amplifiers included a laterally single mode ridge waveguide input with  $4 \dots 5 \mu\text{m}$  ridge width at the rear facet and a separately contacted tapered amplifier section, shown schematically in figure 2. The taper has a flare angle in all cases of  $6^\circ$ , and the facets are passivated for high power operation then dielectric coated for front and rear reflectivities  $R_F = 0.3\%$  and  $R_R = 0.01\%$  respectively (nominal values

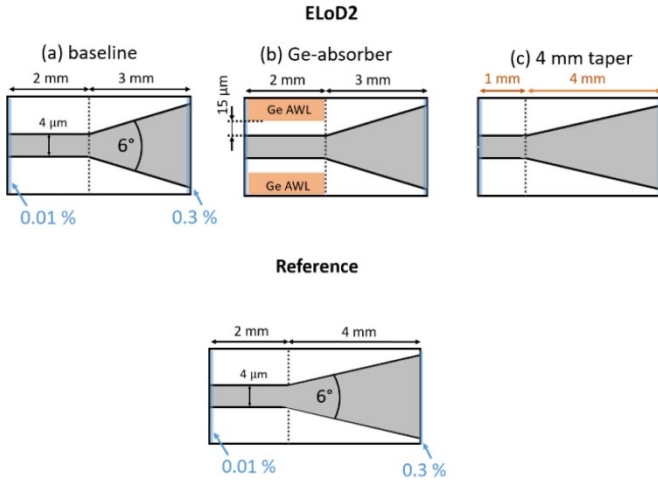


**Figure 2.** Schematic overview of the lateral (in-plane) device geometries tested for the ELOD2 epitaxial design.

based on measured coating layer thicknesses and calculated value of  $n_{\text{eff}}$ ). The baseline lateral design has a taper length  $L_a = 3$  mm and a ridge waveguide length of  $L_{\text{RW}} = 2$  mm. As reported in [19], free-standing tapered lasers with highly reflective rear facets can show improved beam quality and higher  $\eta_{\text{CL}}$  when reverse bias absorber sections are included on either side of the ridge section, to suppress intensity in backwards propagating modes. Even when low facet reflectivities are used, the residual backwards propagating field has been predicted to play a role in limiting beam quality [26], especially when it induces bleaching around the ridge waveguide section, hindering its effectiveness as a mode filter. We therefore assess the benefit here of similar absorber sections on the beam quality, resulting coherent combining efficiency and phase noise, monolithically implemented here using highly absorbing Ge-layers that are designed to resonantly absorb any guided mode, using the designs process reported in [27], which has successfully suppressed higher order lateral modes and improved beam quality in high power broad area lasers. These absorbing regions are located  $15 \mu\text{m}$  laterally offset from the ridge section, as shown in figure 2, equivalent to the location of the reverse-biased absorbers in [19]. Finally, we assess the benefit of larger surface area tapered amplifiers, increasing  $L_a$  to 4 mm for improved cooling and larger single-pass net gain, with reduced ridge waveguide length of  $L_{\text{RW}} = 1$  mm. The reference amplifiers were solely fabricated with  $L_a = 4$  mm and  $L_{\text{RW}} = 2$  mm. All devices were mounted junction-side up onto an expansion matched CuW (10:90) submount, itself soldered onto a C-Mount, with a CuW (10:90) heat spreader soldered onto the tapered section. The C-mount length was matched in each case to the total device length, to retain reasonable cooling and so that both facets were accessible for experiments in single-pass amplifier configuration.

### 3. Comparisons between devices with different vertical and lateral designs

The tapered amplifiers described in the previous section were investigated experimentally in two steps. The characterization

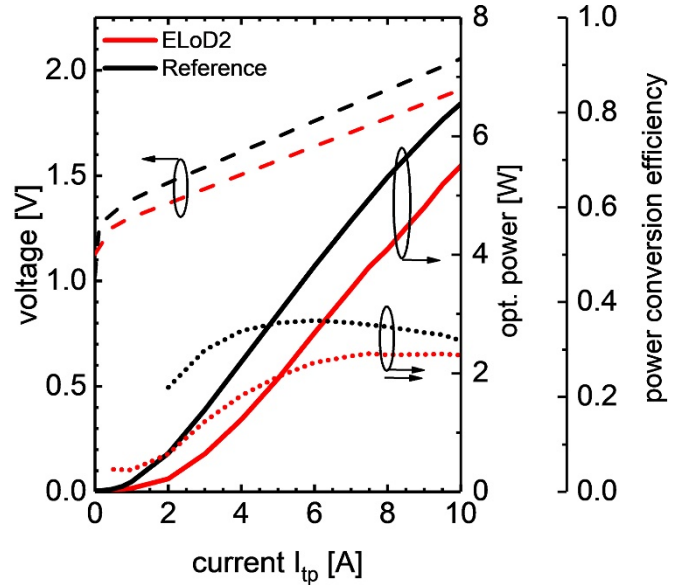


**Figure 3.** Measured CW 20 °C taper voltage (dashed lines), optical output power (solid lines) and conversion efficiency (dotted lines) as a function of taper current under fixed injection conditions ( $P_{\text{in}} = 15\text{--}20$  mW [saturation],  $I_{\text{rw}} = 400$  mA) for reference (black) and ELOD2 (red) tapered amplifiers with  $L_a = 4$  mm.

of individual amplifiers is described in this section in terms of optical output power  $P_{\text{opt}}$  and conversion efficiency (PCE), beam quality and phase noise properties. Three designs were then chosen for simple coherent beam combining experiments described in section 4. A 976 nm distributed feedback (DFB) seed laser diode was used as the seed laser for the following amplifier characterizations. The seed wavelength was consistent and within 10 nm of the peak of the amplified spontaneous emission spectrum, to ensure broadly comparable net gain (the ELOD2 material had  $\sim 9$  nm shorter gain wavelength). The optical isolation and optics used for coupling and collimation were identical to those used in the coherent beam combining setup which is described in detail in section 4.

#### 3.1. Optical output power and conversion efficiency

The electro-optic characteristics of the two investigated epitaxial structures are shown in figure 3, for ridge waveguide current of  $I_{\text{rw}} = 400$  mA and seed power of  $P_{\text{in}} = 15\text{--}20$  mW (sufficient for saturation). Both devices have a  $L_a = 4$  mm long tapered section. We define PCE here in terms of the total output power and the current  $I_{\text{tp}}$  and voltage  $V_{\text{tp}}$  for the tapered amplifier section,  $PCE = P_{\text{opt}}/(I_{\text{tp}} \times V_{\text{tp}})$ . We neglect the contributions of the seed laser and ridge waveguide section, as the power consumed here is small by comparison ( $<5\%$  of total). The optical output power of the reference device was higher than for the ELOD2 amplifier and reached 6.5 W at taper current of  $I_{\text{tp}} = 10$  A ( $PCE_{\text{max}} \approx 36\%$  at  $I_{\text{tp}} = 6$  A). The higher transparency current density for the ELOD2 amplifier (cf section 2.1) leads to an increased turn-on current of the amplifier, which was in the order of 2.5 A for the 4 mm long tapered section device. It results in a reduced optical power of

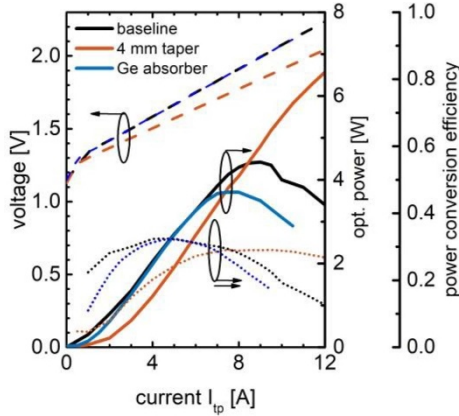


**Figure 4.** Measured CW 20 °C taper voltage (dashed lines), optical output power (solid lines) and conversion efficiency (dotted lines) as a function of taper current under fixed injection conditions ( $P_{in} = 20$  mW [saturation],  $I_{rw} = 400$  mA) for ELoD2 tapered amplifiers with baseline (black), 4 mm taper (red) and Ge-absorber lateral geometry (cf figure 2).

5.5 W at  $I_{tp} = 10$  A and reduced efficiency ( $PCE_{max} \approx 30\%$  at  $I_{tp} = 9.5$  A) when compared to the reference design. The series resistance was however slightly reduced, as evidenced by a slightly lower voltage at high drive currents (cf section 2.1). The slope efficiency was in the order of  $0.7$  W A<sup>-1</sup> for both epitaxial designs for taper bias up to  $I_{tp} = 10$  A.

The electro optic characteristics for ELoD2 amplifiers with the three different lateral (in plane) device configurations are shown in figure 4. Devices with the shorter ( $L_a = 3$  mm) tapered section (baseline and Ge-absorber) showed a low turn-on current in the order of  $I_{tp} = 1.5$  A and a slightly higher power conversion efficiency when compared to the device with  $L_a = 4$  mm. The maximal output power for the baseline design configuration was however limited to 4.4 W by the onset of a thermal rollover at  $I_{tp} = 8$  A. The device configuration with the monolithically integrated Ge-absorber layers suffered from an early thermal rollover at  $I_{tp} = 6$  A attributed to additional losses in the ridge waveguide (RW) section, comparable to those seen in preliminary studies of narrow stripe lasers with Ge-absorber layers [18]. The 4 mm taper device configuration showed the most stable electrooptic characteristics and enabled 6.6 W output power at  $I_{tp} = 12$  A. Indeed the increased area of the tapered section reduces the thermal resistance of the device by a factor of about 40%, and decreases its electrical series resistance too as can be seen on the V(I) evolution. Thus the  $L_a = 4$  mm taper section device can be considered as the most favorable ELoD2 configuration for achieving highest CW powers.

### 3.2. Investigation of the beam quality

The fast axis (FA, vertical) beam quality was nearly diffraction limited for all designs with  $M_{4\sigma}^2 < 1.3$ . The slow axis (SA, lateral, in the plane of the amplifier) beam quality of the different amplifier configurations was investigated using ISO-compliant caustic measurements (second order moments beam diameter) to determine the  $M_{4\sigma}^2$  beam propagation factors and

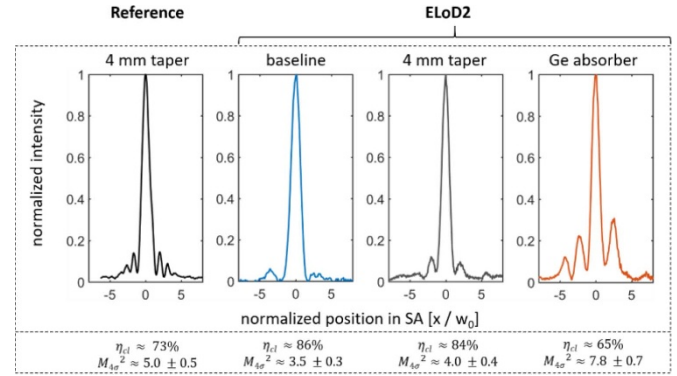


**Figure 5.** Measured CW 20 °C optical intensity as a function of lateral position for images of the lateral beam at the slow-axis waist, for all device configurations assessed (figure 2). Central lobe power content and beam propagation factors are noted, consistent operating conditions are used ( $I_{tp} = 5$  A,  $P_{in} = 15$ –20 mW [saturation],  $I_{rw} = 400$  mA). A normalized lateral length-scale is used, where  $w_0$  corresponds to the  $1/e^2$  radius of the central lobe.

the central lobe power content  $\eta_{cl}$ . Specifically, the central lobe power content was determined by fitting an ideal Gaussian intensity profile to the measured intensity profile at waist (2D analysis) and inferring its power content  $P_{Gauss}$  at a given  $P_{opt}$ , to derive  $\eta_{cl} = P_{Gauss}/P_{opt}$ .

The variation in spatial quality in the horizontal direction (SA) for the various amplifier designs is summarized in figure 5 for an example bias current in the tapered section  $I_{tp} = 5$  A, which is the highest current before thermal rollover effects start to become important. The beam profile for an exemplary single emitter is shown in figure 5, and mean and standard deviation values are given for the beam quality parameters ( $M^2$  and  $\eta_{CL}$ ) taken from several emitters of the same design. The reference design amplifier showed good beam quality with only minor side-lobes at waist, for  $\eta_{cl} = 73\%$ . The most favorable beam quality at this bias point was achieved with the ELoD2 baseline and  $L_a = 4$  mm taper design configurations although as will be shown later, the beam quality of ELoD2 amplifiers with  $L_a = 3$  mm and 4 mm was broadly comparable. In these ELoD2 structures, the central lobe power content was  $>84\%$  and the ISO-compliant beam propagation factor was in the order of 3.5–4.0 in SA, which are excellent values for tapered amplifiers [10, 17] and significantly better than the beam quality achievable with the reference epitaxial design. The design variant including Ge absorber layer showed however poor beam quality in SA with significant side-lobes, appreciably increased beam propagation factor and low central lobe power content. From this comparative study it seems that the monolithically integrated Ge-absorber region deteriorated the beam quality of the tapered amplifier. This conclusion contradicts previous results obtained in both broad area lasers [18, 26] and in free-standing tapered lasers including absorbing regions located on either side of the stripe, that have proven to improve the beam quality of such devices [19].

In order to understand this discrepancy, we experimentally investigated the operation of the RW mode filter in our tapered amplifiers. The RW section is actually critical as its

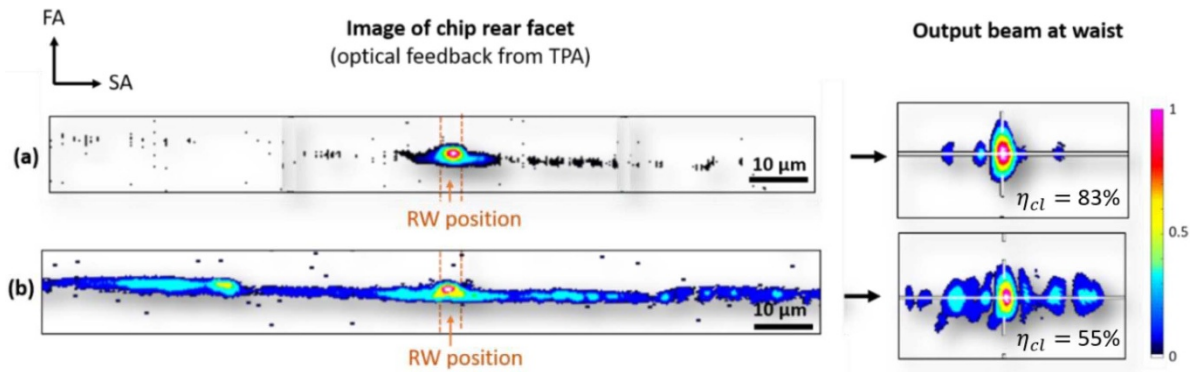


**Figure 6.** Measured spatial distribution of the optical feedback and corresponding output beam at waist (astigmatism corrected) for a normally pumped RW section ( $I_{rw} = 400$  mA), see (a), and an under-pumped RW section ( $I_{rw} = 300$  mA), see (b). Operating conditions:  $I_{ip} = 12$  A,  $P_{in} = 20$  mW,  $T = 20$  °C. An ELoD2 tapered amplifier (4 mm taper design variant) was used. The measurements were taken with identical gain and integration time of the CCD sensor, with intensity normalized and presented as a linearly-scaled false color plot.

role consists in both pre-amplification of the low-power input signal, and in mode filtering. One known explanation for beam quality degradation effects in tapered lasers is the influence of parasitic round-trip effects in the amplifier leading to a dysfunction of the RW mode filter [24–26]. Such parasitic round trip effects can be effectively suppressed by implementing absorber regions on either side of the ridge [16]. Alternatively, DBR gratings can be implemented in the ridge section (to provide the rear-facet optical feedback for round-trip operation) and then anti-reflection coating applied to the rear facet, which strongly suppresses the parasitic-backwards propagating field. It is proposed that the backwards propagating field remains a significant limit to beam quality in single pass-tapered amplifiers [26]. In this case, the backwards propagating amplified spontaneous emission (ASE) field and the field reflected at the output facet (AR coating  $R_F = 0.3\%$ ) have the potential to excite higher-order modes in the ridge, for degraded overall beam quality.

In order to investigate this hypothesis, we made an image of the rear facet of an ELoD2 device with  $L_a = 4$  mm taper under different injection currents into the RW section. Simultaneously we measured the beam profile of the amplified beam at waist. If the RW mode filter works effectively, we would expect the optical feedback signal (at the rear facet) to have a (close-to) Gaussian beam profile corresponding to the fundamental mode guided by the ridge waveguide. This occurs only at the highest injection current  $I_{rw} = 400$  mA (as illustrated in the experimental data shown in figure 6), when the beam quality at the output facet is close to the diffraction limit with high central lobe power content. In contrast, at a lower injection current the optical field spreads over tens of micrometers on both sides of the ridge section, correlating to a poor beam quality of the amplified output beam from the front facet, with multiple side-lobes at waist leading to decreased central lobe power content. This spatial distribution of the optical power on the rear facet of the chip attests that the passive (unbiased) absorbing regions on either side of the RW mode filter are bleached and do not function as an effective filter. It remains however unclear at this point if the observed filter dysfunction is the cause or the effect of the distorted output beam quality.

The various lateral designs of the ELoD2 tapered amplifiers available in this study (cf figure 2) allow the mode filtering properties of the RW section to be further investigated. To this end, the spatial distribution of the beam profile at the rear facet was measured for an un-biased ridge, without using a seed laser ( $I_{rw} = 0$  mA,  $P_{in} = 0$ ). The tapered section was driven under QCW (2 ms, 5 Hz) conditions at moderate current  $I_{ip} = 8$  A (figure 7), with the backward propagating optical field effectively used to excite the guided modes in the ridge waveguide region. The resulting optical fields are shown in figure 7. For both the baseline ( $L_a = 3$  mm, figure 7(b)) and the  $L_a = 4$  mm taper designs (figure 7(c)), the backward ASE is widely spread at the rear facet, far away from the ridge waveguide and the passively absorbing regions around the RW section are strongly bleached. The  $L_a = 4$  mm taper design, with a shorter ridge section and a larger gain volume, delivers a higher ASE-level into the ridge waveguide section, leading to a higher-order lateral mode to be excited (with two lobes), confirming that high levels of backward feedback can degrade the beam in the ridge section, a known cause of poor overall beam quality.

Repeating the same test on devices with Ge-absorber layers clarifies why these devices do not show better overall beam quality. The Ge-absorber layers very effectively absorb the backward propagating ASE across the entire region where they are located (the absorber starts  $\pm 15$   $\mu$ m laterally offset from the RW), and no optical intensity is observed there (see figure 7(a)), in striking contrast to the baseline structure (figure 7(b)). However, an extra laterally two-lobed optical feature is seen in the region between Ge and RW (labelled). We propose that this is either a higher order mode of the RW or an additional or a deformed guided mode naturally arising due to coupling between the Ge-region (with large imaginary refractive index) and the RW. Either effect will degrade the beam quality of the overall system. If the guided modes in the RW are deformed by the use of a Ge-absorber, then high bias of the RW will only have limited benefit on beam quality. Therefore, although the implementation of a Ge-absorber region very effectively suppresses the backward propagating field, we propose that in the process, the modes guided around the ridge

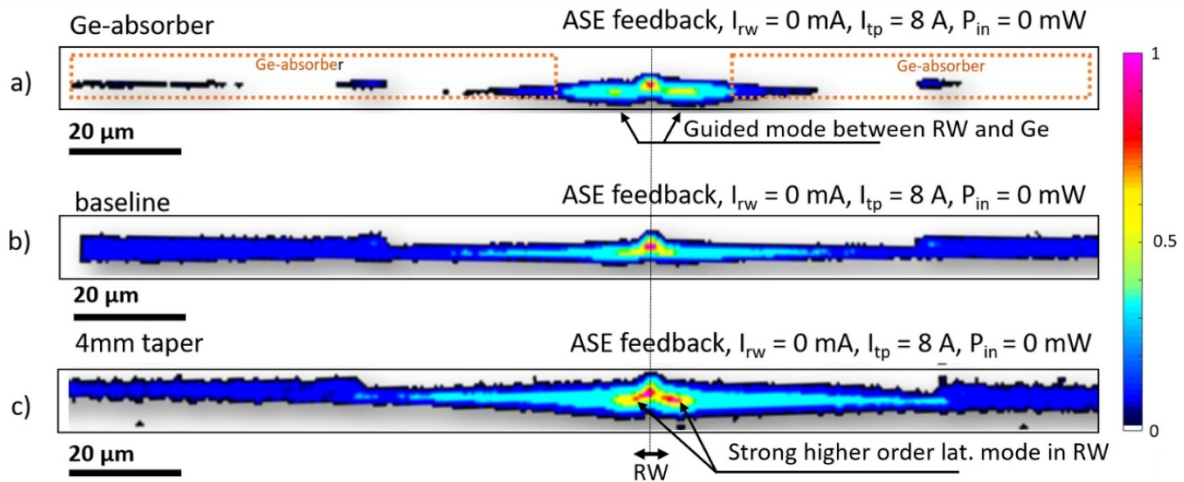


**Figure 7.** Measured spatial distribution of the optical intensity at the chip rear facet, with backwards propagating ASE from the tapered front region used to excite guided modes around the ridge waveguide ( $P_{in} = 0$  mW,  $I_{tp} = 8$  A QCW 2 ms 10 Hz,  $I_{rw} = 0$  mA and  $T = 20$  °C) for three different lateral designs of the ELoD2 tapered amplifier: (a) Ge-absorber, (b) baseline and (c) 4 mm taper (cf figure 2). The measurements were taken with identical gain and integration time of the CCD sensor, with intensity normalized and presented as a linearly-scaled false color plot.

are themselves degraded, leading to poor overall beam quality. Further measurements and simulations would be needed to fully confirm this. Overall, changes in the vertical structure strongly improved the beam quality, attributed to a suppression of filamentation in the tapered section. In contrast, the assessed changes to the lateral structure did not bring any improvement in beam quality, but did help clarify one key additional source of beam degradation—namely, the onset of higher order modes around the ridge section.

### 3.3. Investigation of the phase noise

Operation with low phase noise is essential to achieve and sustain high coherent combining efficiency. Therefore, the phase noise was investigated by injecting a 976 nm seed laser in a simple Mach-Zehnder interferometer, where a tapered amplifier was placed in one arm and a quarter-wave plate was placed in the other arm. In-phase and quadrature components can then be separated at the output of the interferometer allowing the relative phase drift  $\Delta\varphi(t)$  of the two arms in the interferometer to be determined [28]. Figure 8 shows the amplifiers

integrated phase noise spectrum  $S_\varphi(f) = \sqrt{\int_f^{10\text{kHz}} PSD_\varphi(f) df}$ ,

where  $PSD_\varphi(f)$  is the one-sided power spectral density of the measured relative phase drift. A reference measurement, where the tapered amplifier was removed is shown and allows us to determine the phase noise of the external optical setup. The overall noise level is low, dominated by frequencies below 10 Hz and overall comparable to the phase noise in low power single mode ridge waveguide amplifiers [28]. The contribution of the tapered amplifier was in the order of  $\lambda/100$  (integrated from 0.1 Hz to 10 kHz), which is extremely low and can be almost entirely attributed to the temperature stability of the active temperature control (Arroyo 52 400 TEC:  $\Delta T < 0.01$  K). Differences within the different vertical and lateral amplifier designs were in the order of the measurement

precision and there was no evidence for an influence of the device design on the measured phase noise in our study. Note that measurements were done in a well-controlled laboratory environment with minimal influence of external noise sources and that the noise in the interferometer itself may overlay the actual phase noise in the amplifier in other less protected environments. In conclusion one can say that high power tapered amplifiers contribute only marginally to the phase noise in the experimental setup, and any impact of device construction was below measurement accuracy and not significant for device operation. Simple phase control methods with a bandwidth in the order of 100 Hz are more than sufficient to correct the residual phase fluctuations. One straightforward way for phase control in tapered amplifier is an active feedback on the current into the RW of the amplifier as previously demonstrated in [3, 5], which was also used in the coherent beam combining experiments discussed below.

## 4. Coherent beam combining of high brightness amplifiers

The experimental setup used to compare the different amplifier designs in a simple coherent beam combining setup is shown in figure 9 and consists of a two-arm Mach-Zehnder interferometer. A narrow linewidth DFB laser ( $\lambda = 976$  nm, short-time linewidth  $\Delta\nu_{10\ \mu\text{s}} < 20$  MHz,  $P_{out} = 100$  mW) optically isolated by a double stage Faraday isolator (60 dB optical isolation) was used as the master oscillator. The beam was split and recombined by a standard nonpolarising 50:50 beamsplitter. Each amplifier was mounted on a temperature controlled baseplate which supported also the optics for injection into the RW (cf  $L_2$ ), and collimation in FA and SA (cf  $L_3$  and  $L_4$ ). Phase control was achieved by active feedback of the current into the ridge waveguide of one amplifier using a simple

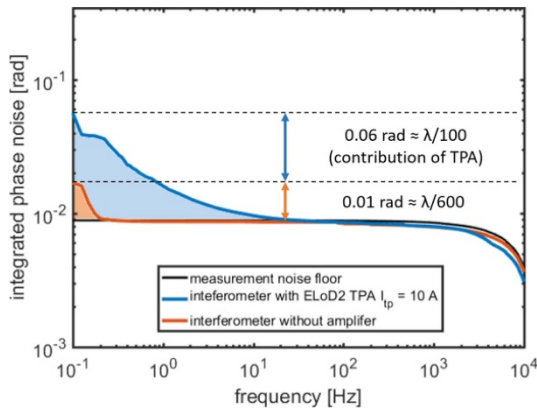


**Figure 8.** Integrated phase noise as function of frequency. Interferometer with tapered amplifier (ELoD2, 4 mm taper config.,  $I_{tp} = 10$  A,  $I_{rw} = 400$  mA,  $P_{in} = 20$  mW) in blue. Reference measurement without amplifier in orange. Measurement noise floor in black.

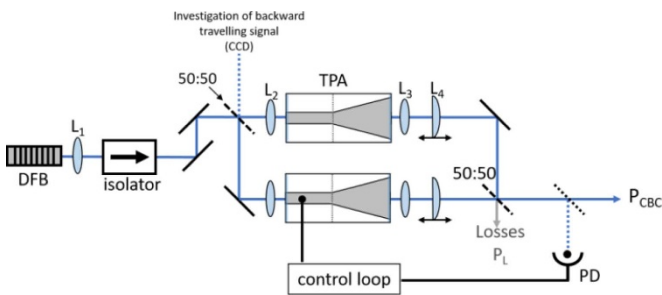


**Figure 9.** Simplified schematic of the experimental setup.  $L_1$  and  $L_2$ : aspherical lens  $f = 8$  mm,  $NA = 0.55$ ;  $L_3$ : aspherical lens  $f = 2.3$  mm,  $NA = 0.55$ ;  $L_4$ : cylindrical lens  $f = 19$  mm. PD: photodiode, TPA: tapered semiconductor optical amplifier. The control loop was implemented using a microcontroller.

hill-climbing algorithm, with  $I_{rw} = 300$ – $400$  mA. The experimental setup was similar to our previously published work on coherent beam combining of tapered amplifiers [5, 6]. In this work, the focus lay on the investigation of factors limiting the combining efficiency (defined as  $\eta_{CBC} = \frac{P_{CBC}}{P_1 + P_2}$ ) by measuring  $\eta_{CBC}$  with the different amplifier configurations. The combining efficiency of two coherent beams is also linked to the spatial overlap factor of the two fields. Beam quality degradation effects lead to non-ideal overlap of the beams and to combining losses [29]. Amplifiers with improved spatial properties enable an improved overlap of the fields, which was experimentally studied here.

The combining efficiency was characterized experimentally at different current levels for tapered amplifiers with the reference epitaxial layer structure and the ELoD2 epitaxial structure. Two lateral design variations were tested for the ELoD2 amplifiers ( $L_a = 3$  mm and 4 mm, devices with Ge-absorber omitted due to poor performance). The results are summarized in figure 10 for the reference epitaxial structure design (black) with the 4 mm-long lateral tapered geometry, the ELoD2 baseline (blue) and the ELoD2 4 mm taper design (red). The reference design enabled high combined output

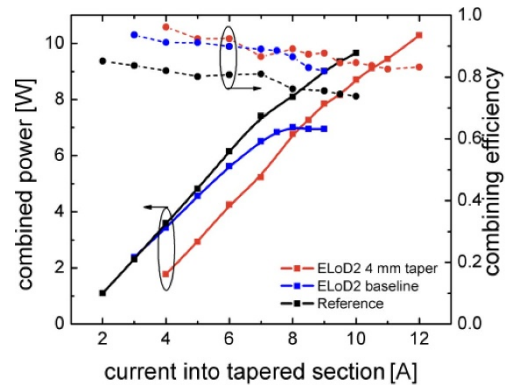


**Figure 10.** Measured CW 20 °C combined output power (solid lines)  $P_{CBC}$  and corresponding combining efficiency  $\eta_{CBC}$  (dotted lines) for CBC of two single-pass tapered amplifiers. Black: reference structure; Blue: ELoD2 baseline geometry; Red: ELoD2 with  $L_a = 4$  mm, under fixed injection conditions ( $P_{in} = 20$  mW [saturation],  $I_{rw} = 300$ – $400$  mA).

power ( $\sim 10$  W at 10 A) but with a moderate combining efficiency (76% at 8 A) that is attributed to the moderate beam quality of the individual amplifiers.

In contrast, figure 10 also shows that the ELoD2 amplifiers allow more efficient coherent beam combining with  $\eta_{CBC} > 84\%$  at 8 A and  $\eta_{CBC} \sim 100\%$  at low currents. No significant difference in combining efficiency was observed for the two different lateral amplifier designs assessed. The ELoD2 devices with baseline taper design ( $L_a = 3$  mm) enables output power comparable to the reference design at low drive currents ( $I_{tp} < 8$  A), the power then however saturated as this amplifier design was limited by an early thermal rollover (cf figure 10). The coherently combined power did not plateau for the 4 mm taper design as expected from the amplifier  $P(I)$  curve in figure 4. The highest combined power of 10.2 W was thus reached with this taper design, in spite of it having the highest turn-on current (largest contact area, high transparency current). It is noteworthy that for both vertical designs the maximum power for coherent beam combining of two amplifiers was similar, but the ELoD2 design achieved 10% higher combining efficiency across the full measured range.

The combining efficiency  $\eta_{CBC}$  is next plotted as a function of the relative central lobe power content  $\eta_{cl}$  of one of the two combined beams as shown in figure 11, corresponding to the measurements in figure 10 ( $\eta_{CL}$  is within 3% for the ELoD2 tapered semiconductor optical amplifiers (TPAs) and for the reference TPAs, so the choice of emitter does not affect the figure). All test data falls onto a single line. Overall, the higher  $\eta_{CBC}$  observed for the ELoD2 tapered amplifiers is solely due to their improved beam quality. Epitaxial design changes, lateral structure changes and changes in device operating condition in this study only affect  $\eta_{CBC}$  to the extent that they influence the beam quality, quantified using  $\eta_{CL}$ . Nonetheless the overall system efficiency  $\eta_{tot} = PCE \times \eta_{CBC}$ , taking into account the PCE of the amplifiers and the combining efficiency, is similar for both the reference (24% at 10 A) and ELoD2 designs (23% at 10 A).

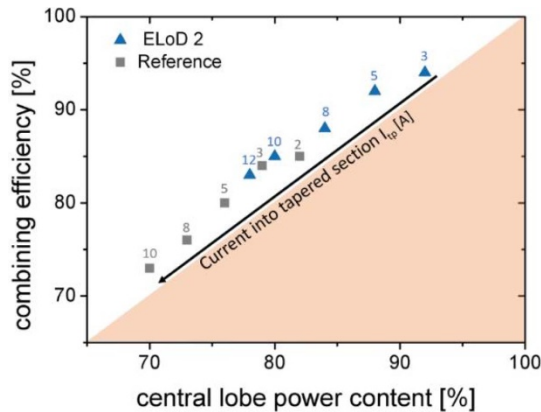


**Figure 11.** Measured combining efficiency  $\eta_{CBC}$  as a function of the central lobe power content  $\eta_{CL}$ . Reference epitaxial structure in gray and ELoD2 4 mm taper design variant in blue, for results taken from figure 11. The corresponding drive current into the tapered section is given in Ampere for each data point.

## 5. Conclusions and next steps

A study was presented into the impact of semiconductor device design on coherent combining in high power single pass tapered amplifiers operating around  $\lambda = 975$  nm. The coherent combining efficiency  $\eta_{CBC}$  was shown to be limited by the beam quality of the amplifier used, with device design and operation mode only relevant to  $\eta_{CBC}$  to the extent that they affect the proportion of power in the diffraction limited central lobe,  $\eta_{CL}$ . Comparison of two epitaxial layer designs shows that ELoD2 structures with extremely low vertical divergence achieve around 10% higher  $\eta_{CL}$  and hence  $\eta_{CBC}$  than a reference design. The improved  $\eta_{CL}$  is proposed as being primarily due to the use of low index quantum barriers, which reduce the impact of variations in the refractive index of the active region on lateral waveguiding. A comparison of lateral taper designs did not lead to increased brightness but did clearly indicate that a high quality single-mode input beam is required, and that any effects that compromise this (for example, onset of higher order modes triggered by back-coupled ASE, or beam deformation triggered by the introduction of highly lossy mode filters) directly degrade  $\eta_{CL}$  and hence  $\eta_{CBC}$ . Phase noise was shown to be low, semiconductor device structure independent (within measurement accuracy), and in no way a limit to coherent combining.

Power per device could be increased by improving thermal resistance (larger area device) or increasing conversion efficiency. Overall, high powered tapered amplifiers were confirmed to be stable, reproducible and robust sources, suitable for use in coherent combining. The high level of stability and reproducibility observed is anticipated to allow coherent combining to be used as a power-scaling tool in many systems, especially those where overall conversion efficiency is not a key factor. Further increases in coherently combined power per device and wider exploitation are expected if the role of the active region in waveguiding can be further suppressed (higher

$\eta_{CL}$ ), if the single mode input section can be more thoroughly protected from the onset of higher order modes (higher  $\eta_{CL}$ ), and if higher conversion efficiency and improved cooling can be achieved (higher power).

## Acknowledgments

We thank Eric Larkins, Hans Wenzel and Bernd Sumpf for many helpful discussions, Jonathan Decker and Martin Winterfeldt for supporting the device measurements, the EU for funding the BRIDLE project, which supported the fabrication of the devices used in this study, the LabEx PALM as part of the ‘Investissements d’Avenir’ program (ANR-10-LABX-0039-PALM) and G Tränkle for his extensive support.

## ORCID iDs

M Elattar  <https://orcid.org/0000-0003-0822-0297>

G Lucas-Leclin  <https://orcid.org/0000-0002-8205-3047>

P Crump  <https://orcid.org/0000-0001-6723-8863>

## References

- [1] Crump P et al 2019 *Advances in High-Power Fiber and Diode Laser Engineering*, ed I Diliansky (Stevenage: IET-Publishing) ch 5
- [2] Fan T Y 2005 *IEEE J. Sel. Top. Quantum Electron.* **11** 567
- [3] Lucas-Leclin G et al 2019 *Advances in High-Power Fiber and Diode Laser Engineering*, ed I Diliansky (Stevenage: IET-Publishing) ch 2
- [4] Vysotsky D V and Napartovich A P 2019 *Quantum Electron.* **49** 989–1007
- [5] Albrodt P et al 2019 *Opt. Express* **27** 928–37
- [6] Albrodt P et al 2019 *Opt. Express* **27** 27891
- [7] Schimmel G et al 2017 *Proc. SPIE* **10086** 100860O–1
- [8] Creedon K J et al 2012 *Opt. Lett.* **37** 5006–8
- [9] Redmond S M et al 2011 *Opt. Lett.* **36** 999–1001
- [10] Wang X et al 2013 *IEEE Photon. Technol. Lett.* **25** 115
- [11] Wenzel H et al 2012 *Proc. SPIE* **8241** 82410V1
- [12] Lang R J et al 1993 *Appl. Phys. Lett.* **62** 1209
- [13] Winterfeldt M et al 2015 *Proc. IEEE Photonics Conf. (Reston, VA, USA, 4–8 October 2015)*, pp 567–8
- [14] Crump P et al 2016 *Proc. SPIE* **9767** 97671L
- [15] Zeghuzi A et al 2019 *IEEE J. Sel. Top. Quantum Electron.* **25** 1502310
- [16] Zeghuzi A et al 2019 *IEEE J. Quantum Electron.* **55** 2000207
- [17] Wang X et al 2012 *Semicond. Sci. Technol.* **27** 015010
- [18] Crump P et al 2015 *Proc. SPIE* **9348** 93480D
- [19] Fiebig C et al 2009 *IEEE Photon. Technol. Lett.* **21** 1755
- [20] Fiebig C et al 2008 *Electron. Lett.* **44** 1253
- [21] Crump P et al 2010 *Appl. Phys. Lett.* **96** 131110
- [22] Crump P et al 2013 *Proc. SPIE* **8605** 86050T
- [23] Bawamia A I et al 2009 *Appl. Phys. B* **97** 95–101
- [24] Bull S et al 2006 *IEE Proc.-Optoelectron.* **153** 2
- [25] Lim J J et al 2009 *IEEE J. Sel. Top. Quantum Electron.* **15** 993
- [26] Helal M A et al 2017 *Handbook of Optoelectronic Device Modeling and Simulation* (Boca Raton, FL: CRC Press) pp 81–108
- [27] Wenzel H et al 2013 *IEEE J. Quantum Electron.* **49** 1102
- [28] Huang R K et al 2009 *Proc. SPIE* **7230** 72301G
- [29] Goodno G et al 2010 *Opt. Express* **18** 25403–14